



Article

Mixed Valence of Ce and Its Consequences on the Magnetic State of Ce₉Ru₄Ga₅: Electronic Structure Studies

Andrzej Ślebarski ^{1,*} , Józef Deniszczyk ²  and Dariusz Kaczorowski ^{3,4} ¹ Institute of Physics, University of Silesia in Katowice, 75 Pułku Piechoty 1, 41-500 Chorzów, Poland² Institute of Materials Engineering, University of Silesia in Katowice, 75 Pułku Piechoty 1A, 41-500 Chorzów, Poland; jozef.deniszczyk@us.edu.pl³ Institute of Molecular Physics, Polish Academy of Sciences, Mariana Smoluchowskiego 17, 60-179 Poznań, Poland; kaczorowski@ifmpan.poznan.pl or d.kaczorowski@intibs.pl⁴ Institute of Low Temperature and Structure Research, Polish Academy of Sciences, PO Box 1410, 50-950 Wrocław, Poland

* Correspondence: andrzej.slebarski@us.edu.pl

Received: 1 May 2020; Accepted: 18 May 2020; Published: 21 May 2020



Abstract: We report on X-ray photoelectron spectroscopy (XPS) and ab initio electronic structure investigations of a novel intermetallic material Ce₉Ru₄Ga₅. The compound crystallizes with a tetragonal unit cell (space group *I4mm*) that contains three inequivalent Ce atoms sites. The Ce 3*d* core level XPS spectra indicated an intermediate valence (IV) of selected Ce ions, in line with the previously reported thermodynamic and spectroscopic data. The ab initio calculations revealed that Ce1 ions located at 2*a* Wyckoff positions possess stable trivalent configuration, whereas Ce2 ions that occupy 8*d* site are intermediate valent. Moreover, for Ce3 ions, located at different 8*d* position, a fractional valence was found. The results are discussed in terms of on-site and intersite hybridization effects.

Keywords: intermetallic Ce compounds; X-ray photoelectron spectroscopy; electronic band structure; hybridization; valence instability; density functional theory

1. Introduction

Physical properties of Ce-based intermetallic compounds are mainly determined by two competing interactions: Kondo effect, characterized by a temperature $T_K \propto \exp(-\frac{1}{|J_{fc}N(E_F)|})$, and Ruderman–Kittel–Kasuya–Yosida (RKKY) interaction, related to $T_{RKKY} \propto J_{fc}^2 N(E_F)$. In both expressions, $N(E_F)$ stands for density of states (DOS) at Fermi level E_F , and $J_{fc} \sim V_{fc}$ is the coupling constant between 4*f* and conduction (c) electron states, where V_{fc} represents on-site hybridization energy given by *f*–*c* hybridization matrix element. According to the Schrieffer–Wolff transformation [1], J_{fc} is defined as $J_{fc} = \frac{2V_{fc}^2}{|E_{4f} - E_F|}$, where E_{4f} stands for energy of 4*f* level. The energy V_{fc} determines filling of the 4*f* shell, and thus governs the character of magnetic ground state. In the Ce-based intermetallics, the hybridization V_{fc} results in a variety of intriguing properties such as heavy-fermion behavior, unconventional superconductivity, various magnetic ordering, non-Fermi liquid, and quantum critical phenomena [2].

For a number of Ce-based compounds reported in the literature, Ce ions occupy a single position in their crystallographic unit cells. If the 4*f*-electron states are strongly localized, i.e., the Kondo interaction is weak, generally, a kind of magnetic ground state is expected. Most often, the compounds order antiferromagnetically, yet, a few ferromagnets are also known, e.g., Ce₂RuGe₂ [3], CeRuPO [4],

Ce₃RhSi₃ [5], CePd₂Al₈ [6], CeCrGe₃ [7], or Ce₁₁Pd₄In₉ [8]. However, the situation becomes less obvious when there is more than a single inequivalent Ce site in the crystal structure. Different local environments of the Ce ions can lead to dissimilar hybridization strengths, which spark the possibility of having distinctly different ground states for each individual inequivalent Ce ion. Recently, investigation of Ce-based compounds bearing multiple inequivalent Ce sites has received considerable attention, and for a few of them, diverse unusual low-temperature properties were established. Prominent examples are Ce₅Ni₆In₁₁, with separate antiferromagnetic orderings in two different Ce atom sublattices [9]; Ce₃Pd₂₀Si₆, with dipolar and quadrupolar antiferromagnetic orders associated with inequivalent Kondo sites [10]; or Ce₃PtIn₁₁ and Ce₃PdIn₁₁, where two different Ce atom sublattices host antiferromagnetism and heavy-fermion superconductivity [11–14].

Another exciting case is the coexistence in a single material of long-range magnetic ordering and valence fluctuations, each phenomenon emerging in a separate Ce atom sublattice. Recently, this very rare situation was reported to occur, e.g., in Ce₂RuGe [15], with two independent Ce atom sites in its crystallographic unit cell, and Ce₉Ru₄Ga₅, which possesses as many as three inequivalent Ce atom sublattices [16,17]. Remarkably, in both compounds one of the different Ce atoms is coordinated by its Ru neighbors at a distance of ~ 2.2 Å and ~ 2.4 Å, respectively, which is much shorter than the sum of the covalent radii of the Ce and Ru atoms. As discussed in detail in a series of our previous papers on the Ce-Ru-X intermetallics (X = Ge, Ga, Al) [15–22], strong Ce–Ru bonding brings about a significant instability of the electronic 4*f* shell, and thus intermediate valence behavior may arise. At the same time, the Ce ions with Ce–Ru distances of regular length remain their trivalent character that promotes localized magnetism with possible magnetic ordering at low temperatures.

The present research was aimed at verification of the electronic character of the particular Ce ions in Ce₉Ru₄Ga₅ by means of X-ray photoelectron spectroscopy and ab initio band structure calculations. Our results fully support the scenario of the dual nature of the 4*f* electrons in this material.

2. Experimental and Computational Details

X-ray photoelectron spectroscopy (XPS) experiments were carried out on a polycrystalline sample Ce₉Ru₄Ga₅ used before for magnetization, magnetic susceptibility, specific heat, and resistivity measurements [17]. The XPS spectra were obtained at room temperature in vacuum of $\sim 10^{-10}$ Torr using a Physical Electronic PHI 5700/600 ESCA spectrometer (Physical Electronics, Inc., Chanhassen, MN, USA) with monochromatized Al K α radiation. The sample was broken in high vacuum of 6×10^{-10} Torr, immediately before the spectra were recorded. Calibration of the spectral data was performed in a manner described in [23]. Binding energies were referenced to the Fermi level ($E_F = 0$).

The electronic band structure of Ce₉Ru₄Ga₅ was calculated using the full-potential linearized augmented plane waves (FP-LAPW) method [24] implemented in the WIEN2k computer code (WIEN2k_18.1, released on 30 June 2018, Institute of Materials Chemistry, TU Viena, Austria) [25] (for details on similarly made computations see, e.g., in [26]). In the performed calculations, we assumed the following electronic configurations of strongly-bound core level states (SC), weakly-bound states (WC), and valence band states in the particular atoms; Ce: [Kr]_{SC}{4*d*¹⁰5*s*²5*p*⁶}_{WC}(4*f*¹5*d*¹6*s*²)_{VB}; Ru: [Ar + 3*d*¹⁰]_{SC}{4*s*²4*p*⁶}_{WC}(4*d*⁷5*s*¹)_{VB}; and Ga: [Ne+3*s*²]_{SC}{3*p*⁶3*d*¹⁰}_{WC}(4*s*²4*p*¹)_{VB}. The fully relativistic formalism was implemented for the SC states, while local orbital (LO) states and VB electrons were treated within the scalar-relativistic Kohn–Sham approach. The spin-orbit (SO) interaction was applied within the second variational approach [24] for calculation of the VB and LO states. The revised Perdew–Burke–Ernzerhof (PBEsol) generalized gradient approximation (GGA) [27] was applied for the exchange correlation (XC) potential.

To determine theoretically the magnetic properties of the individual Ce ions in Ce₉Ru₄Ga₅, the following procedure was applied. First, the PBEsol XC potential was corrected by the Hubbard-like correlation interaction using the approach developed by Anisimov et al. [28,29] with correlation energy parameter $U = 1.5, 2.25, \text{ and } 3$ eV [30]. Then, the ab initio calculations were made within FP-LAPW approach, assuming the muffin-tin (MT) model for crystal potential. The radii of MT spheres, R_{MT} ,

were taken equal 0.121 nm, 0.101 nm, and 0.111 nm for Ce, Ru, and Ga ions, respectively. The accuracy of the performed calculations was determined by the following parameters; $l_{\max} = 10$, $G_{\max} = 14$, and $K_{\max} = 9/R_{\text{MT}} \simeq 8.17 \text{ nm}^{-1}$. A number of $324\vec{k}$ vectors in the irreducible Brillouin zone used in the calculations was found to ensure a total energy convergence of the order of 0.01 eV. The structural data assumed in the initial calculations were taken from work in [16]; however, an atomic relaxation was performed to reach the equilibrium structure. Figure 1 shows the crystal structure of $\text{Ce}_9\text{Ru}_4\text{Ga}_5$, which was the basis for our calculations. In the crystallographic unit cell, there are three inequivalent Wyckoff positions for cerium atoms: $2a$ site with Ce1 atoms, $8d$ site with Ce2 atoms, and another $8d$ site with Ce3 atoms [16]. Throughout the present paper we adopted the Ce atoms labels introduced in Table 2 in Ref. [16]. One should note, however, that in the text of the latter publication and in its figures the Ce1 atom was mistakenly switched with the Ce2 atom (we thank Dr. Elena Murashova, a coauthor of Ref. [16], for giving us comprehensive information about that error).

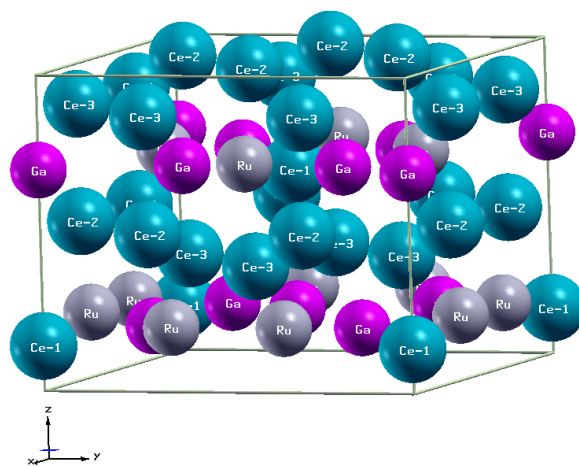


Figure 1. Tetragonal unit cell of $\text{Ce}_9\text{Ru}_4\text{Ga}_5$ (space group $I4mm$, No 107). The structure details are given in Table 1.

3. XPS Results

The X-ray absorption near-edge structure (XANES) spectroscopy, performed for $\text{Ce}_9\text{Ru}_4\text{Ga}_5$ near its Ce L_3 edge, revealed a mixed valence state of the Ce ions, giving an average valence of Ce ions to be about 3.1 at room temperature [16]. In order to corroborate that finding, we measured Ce $3d$ and Ce $4d$ core-level XPS spectra and analyzed the results in terms of the Anderson theory [31]. For a system with partial filling of the Ce $4f$ shell, the theory predicts the appearance of the f^0 and f^2 final states as a result of intra-atomic hybridization between $4f$ and conduction band states. The $3d$ XPS spectrum recorded at room temperature is presented in Figure 2a. The main lines correspond to the $3d_{5/2}^9 4f^1$ and $3d_{3/2}^9 4f^1$ final states, separated by spin-orbit (SO) interaction $\Delta_{\text{SO}} = 18.6 \text{ eV}$. Most remarkably, the spectrum also shows satellites $3d_{5/2}^9 4f^n$ and $3d_{3/2}^9 4f^n$ with $n = 0$ and 2 , separated by the same energy Δ_{SO} .

According to the Gunnarsson–Schönhammer (GS) model [32,33], the $3d 4f^0$ line arises due to the intermediate valence effect, whereas $3d 4f^2$ reflects the on-site hybridization strength, which is expressed by the energy $\Delta_{fc} = \pi V_{fc}^2 N(E_F)$ [31]. It is possible to separate of the overlapping peaks on the basis of the Doniach–Šunjić theory [34], and Δ_{fc} can be estimated from the intensity ratio $I(f^2)/[I(f^1) + I(f^2)]$ of the respective Ce $3d$ XPS lines [33]. In turn, the intensity ratio $r = I(f^0)/[I(f^0) + I(f^1) + I(f^2)]$ gives an estimate for the $4f$ shell mean occupation number n_f [33]. The accuracy of determining Δ_{fc} and n_f is usually less than 20% [35,36] (the limitations were discussed in details, e.g., in [33]). Moreover, one should note that these two quantities are interrelated.

In the case of $\text{Ce}_9\text{Ru}_4\text{Ga}_5$, we found from the GS approach $\Delta_{fc} \approx 210 \text{ meV}$. In order to determine the ground-state $4f$ occupation, we used the theoretical method proposed by Fuggle et al. in Ref. [33],

where the r ratio is calculated as a function of the initial f occupation $c_{(f^0)}$ for different values of Δ_{fc} . Assuming $n_f \approx 1 - c_{(f^0)}$ and $c_{(f^0)}$ equal to wave function amplitude of the initial f^0 configuration state [33], we derived the fractional $4f$ electron count $n_f \approx 0.88$.

The fractional valence of Ce ions in $\text{Ce}_9\text{Ru}_4\text{Ga}_5$ was further corroborated by inspection of the Ce $4d$ XPS spectrum (see Figure 2b), which exhibits two lines near 120 and 124 eV, characteristic of the Ce^{4+} states [33].

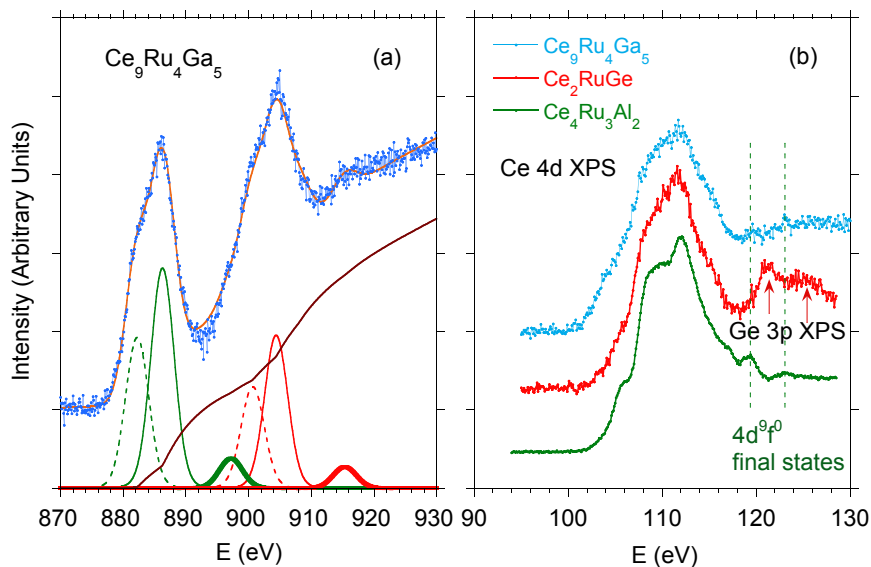


Figure 2. (a) Experimental Ce $3d$ core-level X-ray photoelectron spectroscopy (XPS) spectrum of $\text{Ce}_9\text{Ru}_4\text{Ga}_5$ (blue points) and its Gunnarsson–Schönhammer (GS) modeling (orange line). The contributions $3d_{5/2}^9 4f^n$ and $3d_{3/2}^9 4f^n$ (with $n = 0, 1,$ and 2) are presented in green and red, respectively. The estimated SO splitting is 18.6 eV. The components $3d^9 4f^1$, $3d^9 4f^2$, and $3d^9 4f^0$ are marked by solid, dashed and thick curves, respectively. The brown line represents the calculated background. Panel (b) shows Ce $4d$ XPS spectrum of $\text{Ce}_9\text{Ru}_4\text{Ga}_5$ compared with the respective spectra of the similar intermediate valent compounds Ce_2RuGe and $\text{Ce}_4\text{Ru}_3\text{Al}_2$. For each compound, two features located at 120 and 124 eV (marked by vertical dotted lines) signal mixed valence of Ce ions.

4. Calculated Electronic Structure

The atomic positions in the crystallographic unit cell of $\text{Ce}_9\text{Ru}_4\text{Ga}_5$, obtained as a result of minimizing interatomic forces, are presented in Table 1, and the so-derived local environments of the Ce1, Ce2, and Ce3 atoms are given in Table 2. All the respective interatomic distances are very similar to those reported in the literature [16] (see also Ref. citeremark).

The electronic bands in $\text{Ce}_9\text{Ru}_4\text{Ga}_5$, calculated assuming the correlation energy $U = 1.5$ eV and 2.25 eV, are shown in Figure 3 in a form of the total density of states (TDOS). In addition, the calculations were performed for a model in which different U values were attributed to distinct Ce atoms, and Figure 3 displays the result obtained setting $U = 3$ eV for the Ce1 atom and $U = 2.25$ eV for the Ce2 and Ce3 atoms. As can be inferred from the figure, the DFT data hardly depend on U , except a narrow range of binding energies -1 eV $< E < E_F$. Figure 4a shows the spin-resolved TDOS calculated for the latter values of U compared with the valence band of $\text{Ce}_9\text{Ru}_4\text{Ga}_5$ determined experimentally. Figure 4b, with an expanded energy scale, presents the same theoretical and XPS data together with the partial TDOS due to the particular atoms in the unit cell. Clearly, all the features present in the XPS spectrum are properly reproduced in the computed data. The main contribution due to the Ru $4d$ states is distributed between E_F and the binding energy of 4 eV. In turn, the Ga $4p$ states form bands located near the binding energy of about 6 eV. The Ce $4f$ states are responsible for a broad and fairly weak feature near E_F . At the binding energy of about 17 eV and 19 eV, the calculated

Ce 5*p* electronic states show SO-separated features, which are displaced in respect to the measured data by ~1 eV. The discrepancy can be attributed to Ce 5*d*-electron correlations, which usually shift the calculated Ce 5*p* states to lower binding energies [26,37,38].

Table 1. Relaxed atomic positions in Ce₉Ru₄Ga₅. Calculations were performed assuming the experimental lattice parameters $a = b = 10.1132$ Å and $c = 8.1212$ Å.

Wyckoff	Atom	Coordinates		
Position		x	y	z
2 <i>a</i>	Ce1	0.000000	0.000000	0.141812
8 <i>d</i>	Ce2	0.290732	0.000000	0.498706
8 <i>d</i>	Ce3	0.287464	0.000000	0.871542
8 <i>d</i>	Ru	0.347568	0.000000	0.203546
2 <i>a</i>	Ga1	0.000000	0.000000	0.699153
8 <i>c</i>	Ga2	0.217667	0.217667	0.178952

Table 2. Interatomic distances (Å) in the crystal structure of Ce₉Ru₄Ga₅.

Ce1	Atom	Distance	Ce2	Atom	Distance	Ce3	Atom	Distance
	4Ga2	3.1355		Ru	2.4237		3Ru	2.8233
	Ga1	3.3769		Ce3	3.0114		Ru	2.9531
	4Ce3	3.4661		2Ru	3.0792		Ce2	3.0114
	4Ru	3.6321		2Ce3	3.1721		2Ce2	3.1721
	4Ce2	4.3802		2Ga2	3.2187		Ga1	3.2437
	Ga1	4.7443		Ga1	3.3633		2Ga2	3.2791
				2Ga2	3.5047		2Ga2	3.3838
				Ce2	4.1355		Ce1	3.4661
				2Ce2	4.2269		2Ce3	4.0909
				Ru	4.2978		Ce3	4.3277
				Ce1	4.3802		Ru	4.5993

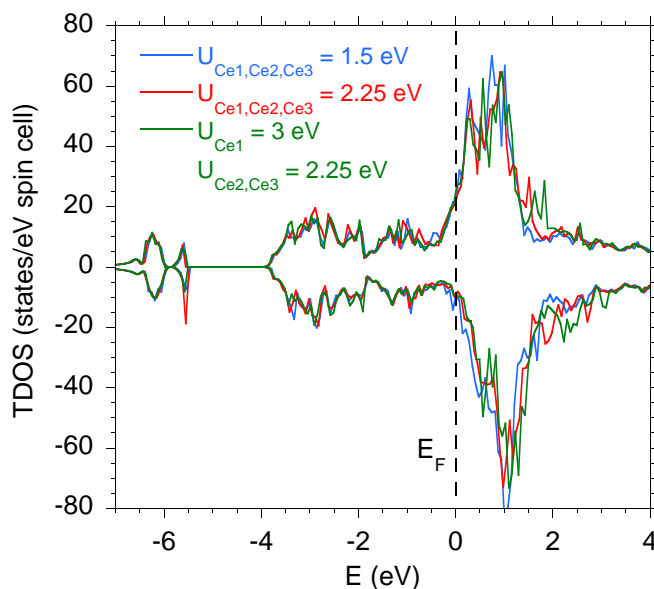


Figure 3. Total spin-resolved density of states in Ce₉Ru₄Ga₅ calculated for different correlation energy parameter U .

The main numerical results of the performed PBEsol+ U calculations are listed in Table 3. For various U , the mean occupancy of the 4*f* shell of the Ce1 atoms is close to 1, while n_f computed for both the Ce2 and Ce3 atoms is notably smaller than 1. The effect of U on the obtained 4*f* electron count is almost negligible. Taking into account the multiplicity of the particular Ce sites, one obtains

an average filling of the 4f shell in $\text{Ce}_9\text{Ru}_4\text{Ga}_5$ equal to 0.86–0.89, in perfect agreement with the experimental result $n_f \approx 0.88$ (see above). The calculated total magnetic moment m_{Ce1} amounts to about $1 \mu_B$, regardless of the value of U , whereas the magnetic moment found at the Ce2 and Ce3 sites is significantly smaller, namely, $m_{\text{Ce2}} \approx 0.3 \mu_B$ and $m_{\text{Ce3}} \approx 0.5 \mu_B$.

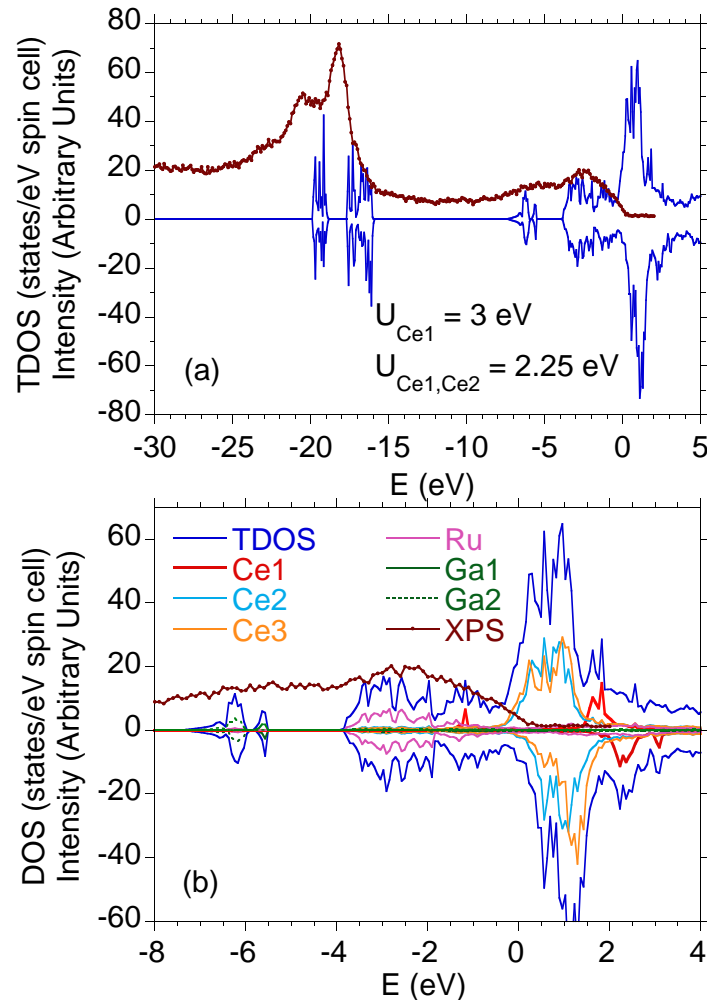


Figure 4. (a) Valence band XPS spectrum of $\text{Ce}_9\text{Ru}_4\text{Ga}_5$ (brown points) compared to the spin-resolved total density of states (blue line) calculated for $U_{\text{Ce1}} = 3 \text{ eV}$ and $U_{\text{Ce2,Ce3}} = 2.25 \text{ eV}$. (b) Total and partial DOS in $\text{Ce}_9\text{Ru}_4\text{Ga}_5$, calculated as in panel (a), compared to the experimental XPS data.

Table 3. Results of the LSDA+U calculations performed for $\text{Ce}_9\text{Ru}_4\text{Ga}_5$ with different values of the correlation energy U , where n_f stands for the number of 4f electrons and m is the total magnetic moment per atom.

$U \text{ (eV)}$		$U_{\text{Ce1,Ce2,Ce3}} = 1.5$		$U_{\text{Ce1,Ce2,Ce3}} = 2.25$		$U_{\text{Ce1}} = 3 \ U_{\text{Ce2,Ce3}} = 2.25$	
$N(E_F) \text{ (eV f.u.)}^{-1}$		31.32		31.32		34.26	
Atom	n_f	$m \text{ (}\mu_B\text{)}$	n_f	$m \text{ (}\mu_B\text{)}$	n_f	$m \text{ (}\mu_B\text{)}$	
Ce1	0.9833	0.9644	0.9880	0.9951	0.9873	1.0149	
Ce2	0.8860	0.2589	0.8446	0.2808	0.8451	0.3099	
Ce3	0.8732	0.4031	0.8309	0.4602	0.8423	0.5295	
Ru		−0.0396		−0.0446		−0.0477	
Ga1		0.0014		0.0023		0.0027	
Ga2		0.0013		0.0024		0.0035	

The fractional valence of the Ce2 and Ce3 ions likely results from the on-site hybridization effect as well as some intersite hybridization between the Ce 4*f* and Ru *d*-electron states. As can be inferred from Figure 5a–c, the on-site *f*–*c* hybridization causes a significant increase in the number of Ce2 and Ce3 5*d*-electron states, whereas the Ce1 4*f* electrons remain well localized at the binding energy of about 1 eV. At the same time, the DFT calculations clearly revealed strong inter-band hybridization of the Ce 5*d* and Ru 4*d* electron states for the Ce2 and Ce3 atoms, whereas the latter effect is negligibly small for the Ce1 atom (see Figure 5d–f).

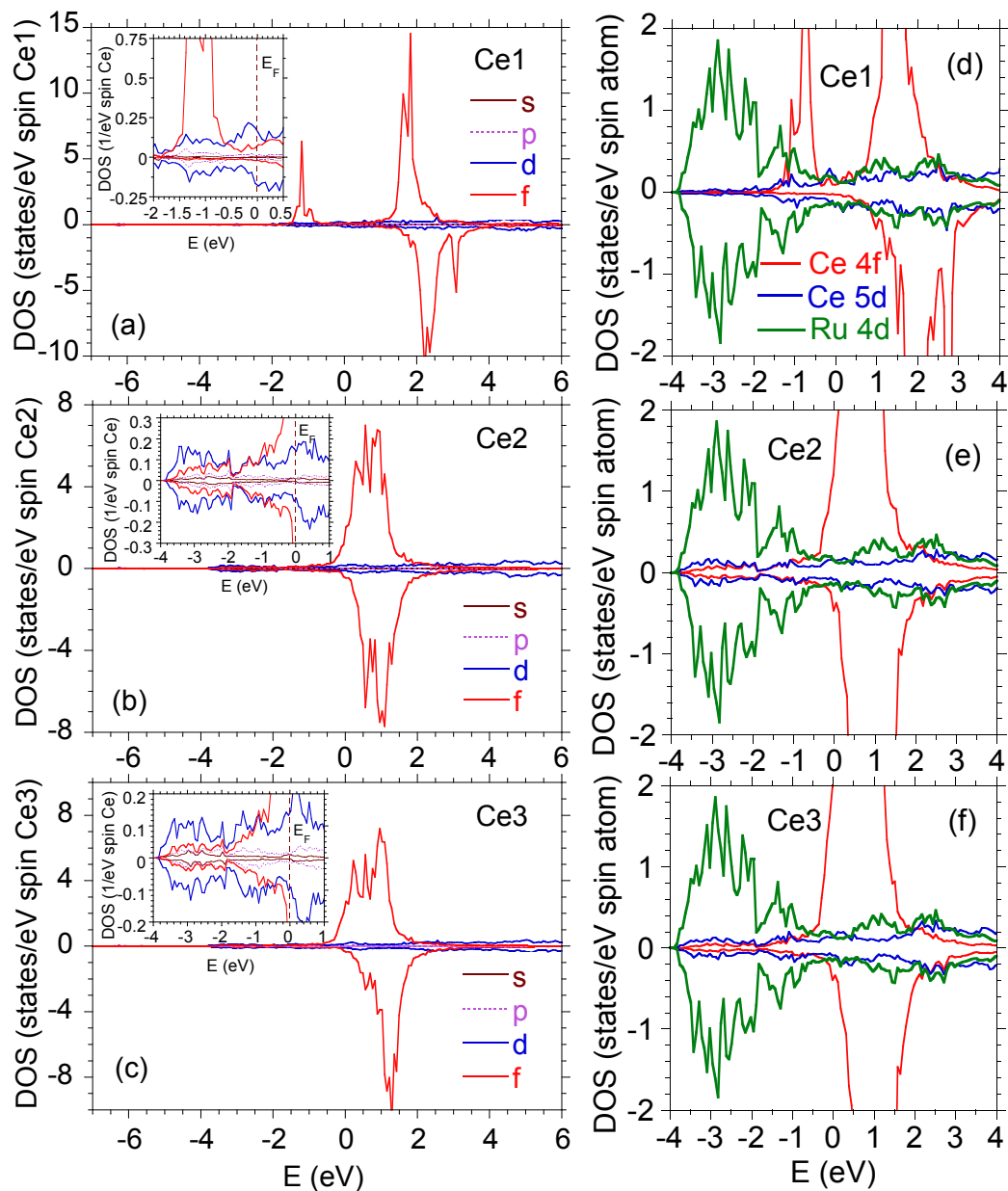


Figure 5. Spin-resolved density of states in $\text{Ce}_9\text{Ru}_4\text{Ga}_5$ due to (a) Ce1, (b) Ce2, and (c) Ce3 atoms. The density of states (DOS) calculations were performed for the correlation parameters $U = 3$ eV for Ce1, and $U = 2.25$ eV for Ce1 and Ce2. The insets present in details the 5*d* contributions. The right panels (d–f) show partial density of states in $\text{Ce}_9\text{Ru}_4\text{Ga}_5$ due to Ce 5*d* and Ru 4*d* electrons at Ce1 (d), Ce2 (e), and Ce3 (f) sites. The DOS calculations were performed for the correlation parameters $U = 3$ eV for Ce1 atom, and $U = 2.25$ eV for Ce2 and Ce3 atoms.

In order to visualize the intersite hybridization and the atomic bonds in the unit cell of $\text{Ce}_9\text{Ru}_4\text{Ga}_5$, we calculated the charge densities (setting $U_{\text{Ce}1} = 3$ eV and $U_{\text{Ce}2,\text{Ce}3} = 2.25$ eV). Figure 6 displays the electron density map within the crystallographic (010) plane. The map clearly shows almost isotropic distribution of valence electrons around the Ce1 and Ga atoms. In contrast, the charge distribution near the Ce2, Ce3, and Ru atoms is strongly anisotropic with strong accumulation of the electronic density along the bonds Ce2-Ru and Ce3-Ru. The strongest covalent bonding occurs between the Ce2 and Ru atoms, in concert with the crystal structure refinement, which revealed abnormally short Ce2-Ru interatomic distance [16]. Thus, the DFT calculations fully corroborated the scenario developed before [16,17], in which the IV behavior in $\text{Ce}_9\text{Ru}_4\text{Ga}_5$, evidenced in the spectroscopic and thermodynamic properties of the compound, can be associated primarily with the Ce2 atoms.

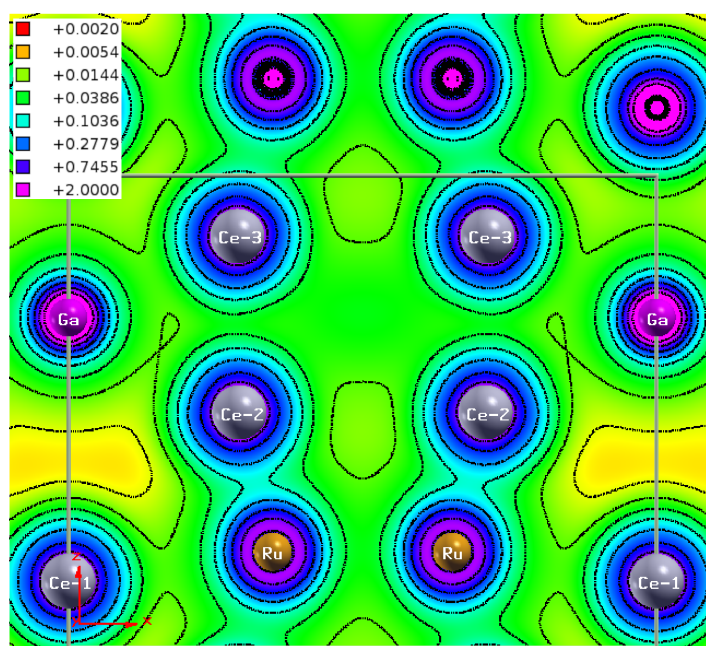


Figure 6. Electron densities $\rho(r)/e$ (in au^{-3}) visualized for the crystallographic plane (010) of the crystal structure of $\text{Ce}_9\text{Ru}_4\text{Ga}_5$. The projection of the unit cell is outlined by gray lines.

5. Conclusions

The XPS experiment performed for $\text{Ce}_9\text{Ru}_4\text{Ga}_5$ confirmed the fractional valence of the Ce ions, noticed before in the L_3 XANES spectroscopy [16] and bulk thermodynamic measurements [17]. The compound forms with a crystallographic unit cell that hosts three inequivalent Wyckoff positions for Ce atoms, thus the experimentally derived filling of the $4f$ shell ($n_f \approx 0.88$) was an average over those three sites. The DFT calculations allowed for inspecting the $4f$ electron counts at each Ce atom. The results indicated that the Ce1 ion located at the $2a$ site is trivalent (n_f is close to 1). In contrast, the Ce2 and Ce3 ions, placed at the $8d$ sites, were found intermediate valent with n_f notably smaller than 1. The ab initio calculated mean occupation of the $4f$ shell in $\text{Ce}_9\text{Ru}_4\text{Ga}_5$ is 0.86–0.89, which is in very good agreement with the experimental finding.

The electronic instability of the $4f$ shell in the Ce2 ion gives rise to the IV character of the compound, established before in the study on its low-temperature bulk physical properties [17]. Most remarkably, the IV features were found to coexist with a long-range antiferromagnetic (AFM) ordering that sets in below $T_N = 3.7$ K [17]. As suggested by our group in an earlier study [17] these two phenomena are spatially separated, i.e., they develop in different Ce ions sublattices. The present DFT results have corroborated such a scenario. Due to dissimilar strength of the intra-site band hybridization, the calculated magnetic moments are distinctly different for Ce1 ($\sim 1 \mu_B/\text{atom}$), Ce2 ($\sim 0.3 \mu_B/\text{atom}$), and Ce3 ($\sim 0.5 \mu_B/\text{atom}$). Therefore, it is reasonable to attribute the AFM state

principally to the Ce1 ions, with a possible contribution due to the Ce3 ions, while the Ce2 ions remain nonmagnetic. The energy $\Delta_{fc} \sim 200$ meV is for Ce₉Ru₄Ga₅ quite large, however, $V_{fc} = (\frac{\Delta_{fc}}{\pi N(E_F)})^{1/2} \sim 44$ meV. One can also estimate the coupling constant $J_{fc} = \frac{2V_{fc}^2}{|E_f - E_F|} \approx 5$ meV [1] between the nearest Ce magnetic moments, which well correlates with low T_N temperature-scale. In order to verify this tempting conjecture, neutron diffraction experiment is compulsory. Undoubtedly, the coexistence of intermediate valent and trivalent cerium ions makes Ce₉Ru₄Ga₅ an interesting material for further comprehensive experimental and theoretical investigations.

Author Contributions: conceptualization, A.Š.; J.D. and D.K.; methodology, A.Š. and J.D.; validation, A.Š.; J.D. and D.K.; formal analysis, A.Š.; investigation, A.Š.; resources, A.Š.; data curation, A.Š.; writing—original draft preparation, A.Š.; writing—review and editing, A.Š.; J.D. and D.K.; visualization, A.Š.; supervision, A.Š., D.K.; project administration, A.Š., D.K.; funding acquisition, A.Š., J.D. All authors have read and agreed to the published version of the manuscript.

Funding: This research received no external funding.

Acknowledgments: We thank Elena Murashova for providing us with a polycrystalline sample of Ce₉Ru₄Ga₅, utilized in the XPS experiment.

Conflicts of Interest: The authors declare no conflict of interest.

References

1. Schieffer, J.R.; Wolff, P.A. Relation between the Anderson and Kondo Hamiltonians. *Phys. Rev.* **1966**, *149*, 491–492. [[CrossRef](#)]
2. Stewart, G.R. Heavy-fermion systems. *Rev. Mod. Phys.* **1984**, *56*, 755–787. [[CrossRef](#)]
3. Boulet, P.; Weitzer, F.; Hiebl, K.; Noel, H. Structural chemistry, magnetic properties and electrical resistivity of the ternary germanides R₂RuGe₂ (R=Y, La, Nd, Gd- Er). *Phys. B Condens. Matter* **2000**, *292*, 302–319. [[CrossRef](#)]
4. Krellner, C.; Kini, N.S.; Bruning, E.M.; Koch, K.; Rosner, H.; Nicklas, M.; Baenitz, M.; Geibel, C. CeRuPO: A rare example of a ferromagnetic Kondo lattice. *Phys. Rev. B* **2007**, *76*, 104418. [[CrossRef](#)]
5. Matusiak, M.; Lipatov, A.; Gribanov, A.; Kaczorowski, D. Anomalous Nernst effect in the ferromagnetic Kondo lattice Ce₃RhSi₃. *J. Phys. Condens. Matter* **2013**, *25*, 265601. [[CrossRef](#)]
6. Tursina, A.; Khamitcaeva, E.; Gnida, D.; Kaczorowski, D. CePd₂Al₈— A ferromagnetic Kondo lattice with new type of crystal structure. *J. Alloys Compd.* **2018**, *731*, 229–234. [[CrossRef](#)]
7. Das, D.; Gruner, T.; Pfau, H.; Paramanik, U.B.; Burkhardt, U.; Geibel, C.; Hossain, Z. Heavy fermion and Kondo lattice behavior in the itinerant ferromagnet CeCrGe₃. *J. Phys. Condens. Matter* **2014**, *26*, 106001. [[CrossRef](#)]
8. Das, D.; Kaczorowski, D. Ferromagnetic Kondo lattice behavior in Ce₁₁Pd₄In₉. *J. Magn. Magn. Mater.* **2019**, *471*, 315–320. [[CrossRef](#)]
9. Tang, J.; Gschneidner, K.A., Jr.; White, S.J.; Roser, M.R.; Goodwin, T.J.; Corruccini, L.R. Ce₅Ni₆In₁₁: An intermediate heavy-fermion system. *Phys. Rev. B* **1995**, *52*, 7328. [[CrossRef](#)]
10. Custers, J.; Lorenzer, K.-A.; Müller, M.; Prokofiev, A.; Sidorenko, A.; Winkler, H.; Strydom, A.M.; Shimura, Y.; Sakakibara, T.; Yu, R.; et al. Destruction of the Kondo effect in the cubic heavy-fermion compound Ce₃Pd₂₀Si₆. *Nat. Mater.* **2012**, *11*, 189. [[CrossRef](#)]
11. Prokleska, J.; Kratochvílova, M.; Uhlířova, K.; Sechovsky, V.; Custers, J. Magnetism, superconductivity, and quantum criticality in the multisite cerium heavy-fermion compound Ce₃PtIn₁₁. *Phys. Rev. B* **2015**, *92*, 161114. [[CrossRef](#)]
12. Das, D.; Gnida, D.; Bochenek, L.; Rudenko, A.; Daszkiewicz, M.; Kaczorowski, D. Magnetic field driven complex phase diagram of antiferromagnetic heavy-fermion superconductor Ce₃PtIn₁₁. *Sci. Rep.* **2018**, *8*, 16703. [[CrossRef](#)] [[PubMed](#)]
13. Kratochvílova, M.; Prokleska, J.; Uhlířova, K.; Tkac, V.; Dusek, M.; Sechovsky, V.; Custers, J. Coexistence of antiferromagnetism and superconductivity in heavy fermion cerium compound Ce₃PdIn₁₁. *Sci. Rep.* **2015**, *5*, 15904. [[CrossRef](#)] [[PubMed](#)]

14. Das, D.; Gnida, D.; Kaczorowski, D. Anisotropic magnetotransport and magnetic phase diagrams of the antiferromagnetic heavy-fermion superconductor $\text{Ce}_3\text{PdIn}_{11}$. *Phys. Rev. B* **2019**, *99*, 054425. [[CrossRef](#)]
15. Kaczorowski, D.; Murashova, E.; Kurenbaeva, Z.; Griбанov, A. Novel germanide Ce_2RuGe : Synthesis, crystal structure and low temperature physical properties. *J. Alloys Compd.* **2019**, *802*, 437–444. [[CrossRef](#)]
16. Shablinskaya, K.; Murashova, E.; Tursina, A.; Kurenbaeva, Z.; Yaroslavtsev, A.; Seropegin, Y. Intermetallics $\text{La}_9\text{Ru}_4\text{In}_5$ and $\text{Ce}_9\text{Ru}_4\text{Ga}_5$ with new types of structure. Synthesis, crystal structures, physical properties. *Intermetallics* **2012**, *23*, 106–110. [[CrossRef](#)]
17. Kaczorowski, D.; Murashova, E.; Kurenbaeva, Z. Antiferromagnetic ordering in an intermediate valence compound $\text{Ce}_9\text{Ru}_4\text{Ga}_5$. *J. Alloys Compd.* **2013**, *557*, 23–26. [[CrossRef](#)]
18. Shablinskaya, K.; Murashova, E.; Kurenbaeva, Z.; Yaroslavtsev, A.; Seropegin, Y.; Kaczorowski, D. Intermetallic compounds $\text{Ce}_4\text{Ru}_3\text{Ga}_3$ and $\text{La}_3\text{Ru}_2\text{Ga}_2$ with crystal structures of new types. *J. Alloys Compd.* **2013**, *575*, 183–189. [[CrossRef](#)]
19. Murashova, E.; Shablinskaya, K.; Kurenbaeva, Z.; Yaroslavtsev, A.; Menushenkov, A.; Chernikov, R.; Grishina, O.; Nesterenko, S.; Seropegin, Y.; Kaczorowski, D. Synthesis, crystal structure and physical properties of $\text{Ce}_2\text{Ru}_2\text{Ga}_3$. *Intermetallics* **2013**, *38*, 23–29. [[CrossRef](#)]
20. Murashova, E.V.; Tursina, A.I.; Bukhanko, N.G.; Nesterenko, S.N.; Kurenbaeva, Z.M.; Seropegin, Y.D.; Noel, H.; Potel, M.; Roisnel, T.; Kaczorowski, D. New ternary intermetallics $\text{RE}_5\text{Ru}_3\text{Al}_2$ (RE = La, Ce, Pr): synthesis, crystal structures, magnetic and electric properties. *Mater. Res. Bull.* **2010**, *45*, 993–999. [[CrossRef](#)]
21. Marushina, E.V.; Kaczorowski, D.; Murashova, E.V.; Kurenbaeva, Z.M.; Griбанov, A.V. Crystal structure and unstable valence in a novel intermetallic phase $\text{Ce}_2\text{Ru}_2\text{Al}$. *J. Alloys Compd.* **2015**, *650*, 654–657. [[CrossRef](#)]
22. Murashova, E.; Kurenbaeva, Z.; Tursina, A.; Marushina, E.; Yaroslavtsev, A.; Leshchev, D.; Seropegin, Y.; Kaczorowski, D. Novel ternary compound Ce_2RuAl : synthesis, crystal structure, magnetic and electrical properties. *J. Alloys Compd.* **2013**, *580*, 55–60. [[CrossRef](#)]
23. Baer, Y.; Bush, G.; Cohn, P. Monochromatized X-ray source for high-resolution electron-spectroscopy. *Rev. Sci. Instrum.* **1975**, *46*, 466–469. [[CrossRef](#)]
24. Singh, D.J.; Nordstrom L. *Plane Waves, Pseudopotentials, and the LAPW Method*, 2nd ed.; Springer Science: Berlin, Germany 2006; ISBN 978-0-387-28780-5.
25. Blaha, P.; Schwarz, K.; Madsen, G.K.H.; Kvasnicka, D.; Luitz, J.; Laskowski, R.; Tran, F.; Marks, L.D. WIEN2k. In *An Augmented Plane Wave + Local Orbitals Program for Calculating Crystal Properties*; Schwarz, K., Ed.; Techn. Universität Wien: Vienna, Austria, 2001; ISBN 3-9501031-1-2.
26. Ślebarski, A.; Deniszyk, J.; Murashova, E.; Kaczorowski, D. Magnetic ground state in novel valence fluctuating compound Ce_2RuGe : Electronic structure investigations. *J. Magn. Magn. Mater.* submitted.
27. Perdew, J.P.; Ruzsinszky, A.; Csonka, G.I.; Vydrov, O.A.; Scuseria, G.E.; Constantin, L.A.; Zhou, X.; Burke, K. Restoring the Density-Gradient Expansion for exchange in solids and surfaces. *Phys. Rev. Lett.* **2008**, *100*, 136406. [[CrossRef](#)] [[PubMed](#)]
28. Anisimov, V.I.; Zaanen, J.; Andersen, O.K. Band theory and Mott insulators: Hubbard U instead of Stoner I. *Phys. Rev. B* **1991**, *44*, 943–954. [[CrossRef](#)]
29. Anisimov, V.I.; Solovyev, I.V.; Korotin, M.A.; Czyżyk, M.T.; Sawatzky, G.A. Density-functional theory and NiO photoemission spectra. *Phys. Rev. B* **1993**, *48*, 16929–16934. [[CrossRef](#)] [[PubMed](#)]
30. Fabris, S.; de Gironcoli, S.; Baroni, S.; Vicario, G.; Balducci, G. Taming multiple valency with density functionals: A case study of defective ceria. *Phys. Rev. B* **2005**, *71*, 041102. [[CrossRef](#)]
31. Anderson, P.W. Localized magnetic states in metals. *Phys. Rev.* **1961**, *124*, 41–53. [[CrossRef](#)]
32. Gunnarsson, O.; Schönhammer, K. Electron spectroscopies for Ce compounds in the impurity model. *Phys. Rev. B* **1983**, *28*, 4315–4341. [[CrossRef](#)]
33. Fuggle, J.C.; Hillebrecht, F.U.; Zolnieriek, Z.; Lässer, R.; Freiburg, Ch.; Gunnarsson, O.; Schönhammer, K. Occupancy and hybridization of the f level in Ce compounds. *Phys. Rev. B* **1983**, *27*, 7330–7341. [[CrossRef](#)]
34. Doniach, S.; Šunjić, M. Many-electron singularity in X-ray photoemission and X-ray line spectra from metals. *J. Phys. C* **1970**, *3*, 285–291. [[CrossRef](#)]
35. Ślebarski, A.; Radłowska, M.; Zawada, T.; Maple, M.B.; Jezierski, A.; Zygumnt A. Experimental study of the physical properties in the complex magnetic phase diagram of $\text{Ce}_{1-x}\text{Rh}_x\text{RhSn}$. *Phys. Rev. B* **2002**, *66*, 104434. [[CrossRef](#)]
36. Ślebarski, A.; Zawada, T.; Spalek, J.; Jezierski, A. Effect of Sn doping on the coherent Kondo gap and emergence of a non-Fermi-liquid state in $\text{CeRhSb}_{1-x}\text{Sn}_x$. *Phys. Rev. B* **2004**, *70*, 235112. [[CrossRef](#)]

37. Ślebarski, A.; Gorau, J.; Witas, P.; Kalinowski, L.; Fijałkowski, M. Study of d-electron correlations in skutterudite-related $Ce_3M_4Sn_{13}$ (M=Co, Ru, and Rh). *Phys. Rev. B* **2015**, *91*, 035101. [[CrossRef](#)]
38. Skornia, P.; Deniszczyk, J.; Fijałkowski, M.; Ślebarski, A. Coexistence of ferromagnetic-type order and spin-glass-like behavior in Ce_5AgGe_2 . *J. Alloys Compd.* **2019**, *790*, 1051–1059. [[CrossRef](#)]



© 2020 by the authors. Licensee MDPI, Basel, Switzerland. This article is an open access article distributed under the terms and conditions of the Creative Commons Attribution (CC BY) license (<http://creativecommons.org/licenses/by/4.0/>).